Direct evidence for high affinity blockade of Nav1.6 channel subtype by huwentoxin-IV spider peptide, using multiscale functional approaches

Tânia C. Gonçalves, Rachid Boukaiba, Jordi Molgó, Muriel Amar, Michel Partiseti, Denis Servent, Evelyne Benoit

Direct evidence for high affinity blockade of $Na_V1.6$ channel subtype by huwentoxin-IV spider peptide, using multiscale functional approaches

Tânia C. Gonçalves [a,b], Rachid Boukaiba [a], Jordi Molgó [b,c], Muriel Amar [b], Michel Partiseti [a], Denis Servent [b], Evelyne Benoit [b,c,*]

[a] *Sanofi Aventis R & D, Integrated Drug discovery - In Vitro Biology & Pharmacology, F-94440 Vitry-sur-Seine, France*

[b] *Service d'Ingénierie Moléculaire des Protéines (SIMOPRO), CEA, Université Paris-Saclay, F-91191 Gif sur Yvette, France*

[c] *Institut des Neurosciences Paris-Saclay (Neuro-PSI), UMR CNRS/Université Paris-Sud 9197, Université Paris-Saclay, F-91198 Gif sur Yvette, France*

* Corresponding author. Current address: CEA de Saclay, SIMOPRO, Bât. 152, 91191 Gif-sur-Yvette, France. Tel: +33-1-69-08-56-85. Fax: +33-1-69-08-90-71

E-mail address: evelyne.benoit@cea.fr (E. Benoit).

Running title: Huwentoxin-IV and $Na_V1.6$ channel subtype

Highlights

- HwTx-IV inhibits *in vivo* nerve-elicited compound muscle action potential in mice
- HwTx-IV blocks *in vitro* nerve- and not directly-evoked mouse muscle contraction
- HwTx-IV preferentially blocks TTX-S Na_V subtypes overexpressed in HEK-293 cells
- HwTx-IV is more potent to block TTX-S than TTX-R Na_V channels of mouse DRG neurons

Ethical statement. All efforts were made to minimise the suffering of mice, and a minimal number of animals was used. All experimental procedures were carried out in accordance with the guidelines established by the French Council on animal care "Guide for the Care and Use of Laboratory Animals" (EEC86/609 Council Directive – Decree 2001-131), and the experimental protocols were approved on November 27 2015 by the French General Directorate for Research and Innovation (project APAFIS#2671-2015110915123958v3 authorized to E.B.).

ABSTRACT

The Chinese bird spider huwentoxin-IV (HwTx-IV) is well-known to be a highly potent blocker of $Na_V1.7$ subtype of voltage-gated sodium (Na_V) channels, a genetically validated analgesic target, and thus promising as a potential lead molecule for the development of novel pain therapeutics. In the present study, the interaction between HwTx-IV and $Na_V1.6$ channel subtype was investigated using multiscale (from *in vivo* to individual cell) functional approaches. HwTx-IV was approximatively 2 times more efficient than tetrodotoxin (TTX) to inhibit the compound muscle action potential recorded from the mouse skeletal neuromuscular system *in vivo*, and 30 times more effective to inhibit nerve-evoked than directly-elicited muscle contractile force of isolated mouse hemidiaphragms. These results strongly suggest that the inhibition of nerve-evoked skeletal muscle functioning, produced by HwTx-IV, resulted from a toxin-induced preferential blockade of $Na_V1.6$, compared to $Na_V1.4$, channel subtype. This was confirmed by whole-cell automated patch-clamp experiments performed on human embryonic kidney (HEK)-293 cells overexpressing $hNa_V1.1$-1.8 channel subtypes. HwTx-IV was also approximatively 850 times more efficient to inhibit TTX-sensitive than TTX-resistant sodium currents recorded from mouse dorsal root ganglia neurons. Finally, based on our data, we predict that blockade of the $Na_V1.6$ channel subtype was involved in the *in vivo* toxicity of HwTx-IV, although this toxicity was more than 2 times lower than that of TTX. In conclusion, our results provide detailed information regarding the effects of HwTx-IV and allow a better understanding of the side-effect mechanisms involved *in vivo* and of channel subtype interactions resulting from the toxin activity.

Keywords: huwentoxin-IV, voltage-gated sodium channels, Na_V channel subtypes, electrophysiology, mouse neuromuscular excitability, mouse dorsal root ganglia neurons, cell lines overexpressing Na_V channel subtypes

Abbreviations

Ca_V channel	voltage-gated calcium channel
CHO	Chinese hamster ovary
CMAP	compound muscle action potential
DMEM	Dulbecco's modified Eagle's medium
DRG	dorsal root ganglia
ERG	*ether-a-go-go*-related gene
h	human
HEK	human embryonic kidney
HEPES	N-2-hydroxyethylpiperazine-N'-2-ethanesulfonic acid
HwTx-IV	huwentoxin-IV
i.m.	intramuscular
IC_{50}	toxin concentration necessary to inhibit 50% of the response
ICK	inhibitory cystine knot
K_V channel	voltage-gated potassium channel
NaSpTx	voltage-gated sodium channel spider toxin
Na_V channel	voltage-gated sodium channel
PBS	phosphate buffered saline
ProTx-II	protoxin-II
r	rat
TTX	tetrodotoxin
TTX-R	resistant to tetrodotoxin
TTX-S	sensitive to tetrodotoxin

1. Introduction

Pain treatment diversification remains a big health and economic concern, and animal venom peptides seem to be an original source of new antinociceptive drugs targeting ion channels implicated in pain signalling pathways. Their modest size, compact structure due to disulfide bridges, physicochemical resistance to enzyme degradation and tissue clearance make them good candidates (Saez et al., 2010). A FDA-approved painkiller is already commercialized as Prialt® since a decade. This peptide derived from a conus venom toxin, blocks the $Ca_V2.2$ subtype (N-type) of voltage-gated calcium (Ca_V) channels to relieve chronic pain of spinal cord injury non treatable by opioid therapy (Molinski et al., 2009). Unfortunately, the peptide administered *via* intrathecal injection induces severe side-effects which restrain its wider application (Wang et al., 2016). Even if Prialt® is still the only venom-derived drug approved for pain treatment, many other toxins entered in pre-clinical or clinical development due to their capacity to interact with major molecular targets of pain pathways, such as sodium, calcium, and acid-sensing ion channels, as well as nicotinic receptors (Netirojjanakul and Miranda, 2017).

Due to their major role in initiating and propagating action potentials, voltage-gated sodium (Na_V) channels are implicated in numerous pain diseases. Some of these diseases can be directly linked to mutations of genes encoding the $Na_V1.7$ channel subtype, leading to either exacerbation of pain, such as inherited erythromelalgia, paroxysmal extreme pain disorder and small fiber neuropathy, or no pain sensation at all, such as congenital insensitivity to pain or type-IID hereditary sensory and autonomic neuropathy (de Lera Ruiz and Kraus, 2015; Vetter et al., 2016). Na_V channels are transmembrane proteins composed of a pore-forming α subunit constituted by four domains, each containing 6 transmembrane segments, the S1-S4 forming the voltage-sensing domain and the S5 connected to the S6 with an extracellular re-entrant P-loop constituting the ion-conducting pore (Goldin et al., 2000; Catterall, 2000; de Lera Ruiz and Kraus, 2015). The gating properties and turnover of Na_V channels may be modified by some members of the cell adhesion molecule superfamily, the β subunits, linked to the α subunit (Namadurai et al., 2015).

More than ten toxins have been reported so far to act selectively and potently

on $Na_V1.7$ channel subtype (Vetter et al., 2016). Among these toxins, protoxin-II (β/ω-theraphotoxin-Tp2a or ProTx-II) and huwentoxin-IV (μ-theraphotoxin-Hs2a or HwTx-IV) have been well characterized (Xiao et al., 2014). HwTx-IV, extracted from the venom of the Chinese bird spider *Cyriopagopus schmidti*, formerly known as *Haplopelma schmidti* (Schmidt, 2010), is a 35 amino acid peptide, with an inhibitory cystine knot (ICK) architectural motif, belonging to Na_V channel spider toxin (NaSpTx) family 1 (Klint et al., 2012). HwTx-IV was first identified as a highly potent blocker of the genetically validated analgesic target $Na_V1.7$ channel subtype, showing in addition a marked selectivity for this channel subtype compared, in particular, to the heart channel subtype $Na_V1.5$ and the skeletal muscle channel subtype $Na_V1.4$ which were relatively resistant to the peptide (Xiao et al., 2008). Great efforts were then provided to link the promising toxin to an antinociceptive effect *via* Na_V channels. The first report introduced the toxin as having a high efficacy on tetrodotoxin (TTX)-sensitive Na_V channels located in rat dorsal root ganglia (DRG) neurons [toxin concentration necessary to inhibit 50% of the response (IC_{50}) of 30 nM] which are involved in pain pathway (Peng et al., 2002). More recently, HwTx-IV was reported to have analgesic effects in rodent inflammatory and neuropathic pain models (Liu et al., 2014a). The peptide was thus promising as a potential lead molecule for the development of novel pain therapeutics. However, until now, very few information was reported about the efficiency of HwTx-IV to interact with the $Na_V1.6$ channel subtype, a TTX-sensitive (TTX-S) Na_V channel subtype present in the brain, in DRG neurons and in Ranvier nodes of α–motoneurons, as well as the resulting *in vivo* side-effects resulting from this interaction (Rahnama et al., 2017). This point is very important since such interaction would, in particular, impair the neuromuscular system functioning, leading to the death of experimental animals, as previously suggested (Liu et al., 2014b; Flinspach et al., 2017; Rahnama et al., 2017; Deuis et al., 2016).

The present study was therefore undertaken to determine the interaction between HwTx-IV and $Na_V1.6$ channel subtype, using multiscale (from *in vivo* to individual cell) functional approaches. Our results provide detailed information regarding the effects of the peptide on the mouse neuromuscular system *in vivo*, on isolated mouse neuromuscular preparations, on mouse DRG neurons and on human embryonic kidney (HEK)-293 cells heterologously overexpressing the human (h)

$Na_V1.6$ channel subtype, therefore providing a clue to understand the mechanisms of *in vivo* motor side-effects resulting from HwTx-IV and $Na_V1.6$ channel subtype interaction.

2. Material and methods

2.1. Toxins

Lyophilized synthetic HwTx-IV (molecular weight of 4106.811, purity rate > 97%) was obtained from Smartox Biotechnology (Saint Martin d'Hères, France). This toxin was dissolved in phosphate buffered saline (PBS 1X) solution to give a 2.5×10^{-2} g/mL (*i.e.* 6.1 mM) stock solution. TTX citrate (molecular weight of 319.27, purity rate > 98%) was purchased from Sigma-Aldrich (Saint-Quentin Fallavier, France). This toxin was dissolved in PBS 1X solution to give a 9×10^{-4} g/mL (*i.e.* 2.85 mM) stock solution. Just prior to experiments, successive dilutions were performed in the adequate standard physiological medium to give the HwTx-IV and TTX final concentrations indicated in the text.

2.2. Experimental animals

Adult female Swiss mice (10-12 weeks of age and 28-32 g body weight) were purchased from Janvier Elevage (Le Genest-Saint-Isle, France) and housed at the CEA animal facility. The experiments were performed in accordance with the guidelines established by the French Council on animal care "Guide for the Care and Use of Laboratory Animals" (EEC86/609 Council Directive – Decree 2001-131), on mice under anaesthesia by means of isoflurane (AErrane®, Baxter S.A., Lessines, Belgique) inhalation. The experimental protocols were approved on November 27 2015 by the French General Directorate for Research and Innovation (project APAFIS#2671-2015110915123958v3 authorized to E.B.).

2.3. Isolated mouse neuromuscular preparations

Mouse hemidiaphragms with their respective associated phrenic nerve were rapidly and carefully dissected after anaesthesia (by isoflurane inhalation) and euthanasia (by cervical vertebrae dislocation) of mice. After removal, the isolated neuromuscular preparation was mounted on a silicone-lined organ bath (4 mL

volume) filled with a standard physiological medium of the following composition (in mM): NaCl 145, KCl 5, $CaCl_2$ 2, $MgCl_2$ 1, D-glucose 11, and N-2-hydroxyethylpiperazine-N'-2-ethanesulfonic acid (HEPES) 5 (pH 7.4, adjusted with NaOH), continuously gassed with pure O_2 throughout the experiment.

2.4. Primary cultures of mouse DRG neurons

Mouse DRG were removed from the animal spinal cord, placed in iced-Ham's F-12 medium (Sigma-Aldrich) and enzymatically dissociated with collagenase type IA (2 mg/mL; Sigma-Aldrich) and dispase (5 mg/mL; Gibco, Thermo Fisher Scientific, Villebon-sur-Yvette, France). Neurons were then plated on 12-mm glass coverslips placed in a 24-wells plate coated with 10 µg/mL of poly-D-lysine and 100 µg/mL of murin laminin (Sigma-Aldrich). The cells were maintained in culture at 37°C (in 95% air and 5% CO_2) in Neurobasal A medium (Gibco) containing horse serum (5%; Gibco), penicillin/streptomycin (47.64 U/mL; Gibco), nerve growth factor (83.33 ng/mL; Sigma-Aldrich), N2 supplement (3.18x; Gibco), Dulbecco's phosphate-buffered saline (1X) w/o $CaCl_2$ and $MgCl_2$ (1.68%; Gibco), bovine serum albumin (16.83 µg/mL; Sigma-Aldrich), corticosteron (214.85 nM; Sigma-Aldrich), T3 hormone (56.06 nM; Sigma-Aldrich) and L-glutamine (1.90 mM; Sigma-Aldrich). Cytosine β-D-arabinofuranoside (2 µM; Sigma-Aldrich) was added to the culture medium, 24 hours later, to stop astrocyte proliferation.

Experiments were carried out within 2 to 6 days after cell plating. The day of their use, the neurons plated on coverslips were transferred, for a minimum of 30 min at 37°C prior to manual patch-clamp recordings, in 35-mm Petri dishes filled with a standard physiological medium of the following composition (in mM): NaCl 134, KCl 3, $CaCl_2$ 1, $MgCl_2$ 1, D-glucose 10, tetraethylammonium chloride (TEA) 10, $CdCl_2$ 0.1, and HEPES 10 (pH 7.35, adjusted with NaOH), and then in the recording bath filled with the standard physiological medium.

2.5. HEK-293 and Chinese hamster ovary (CHO) cell line cultures

HEK-293 cells heterologously overexpressing $hNa_V1.7$ (Eurofins, Discovery Services, St Charles, MO, USA) were cultured in suspension in FreestyleTM293 (Gibco; #12338-018). Those overexpressing $hNa_V1.1$ (Eurofins), $hNa_V1.6$ (ChanTest, Cleveland, OH, USA) or $hNa_V1.8$ (Millipore, Billerica, MA, USA) were cultured in

Dulbecco's modified Eagle's medium (DMEM)/F-12 nutrient mixture with GlutaMAX™ supplement (Gibco; #31331), those overexpressing $hNa_V1.2$ (SB Drug Discovery, Glasgow, United Kingdom) and $hNa_V1.5$ (Sanofi, Frankfurt, Germany) in DMEM with GlutaMAX™ supplement (Gibco; #31966), and those overexpressing $hNa_V1.3$ and 1.4 (SB Drug Discovery) in minimum essential medium (Sigma-Aldrich; #M5650). CHO cells heterologously overexpressing $hCa_V1.2/\beta2/\alpha2\delta1$ (ChanTest, Cleveland, OH, USA) were cultured in Ham's F12 nutrient mix with GlutaMAX™ medium (Gibco; #31765). Those overexpressing the voltage-gated potassium (K_V) channel subtype $hK_V11.1$ (B'SYS GmbH, Switzerland), encoded by the human *ether-a-go-go*-related gene (hERG), were cultured in DMEM/F-12 nutrient mixture Ham's medium (Sigma; #D6434). All culture media contained fetal bovine serum (10% v/v) and selected antibiotics and additives, as recommended by the manufacturer. Cells were grown in flasks, in a humidified 5% CO_2 incubator at 37°C, and subcultured/passaged every 3-4 days using TrypLE Select enzyme (Gibco).

For manual patch-clamp recordings, a few days before experiments, the cells were transferred on 12-mm glass coverslips placed in 35-mm Petri dishes. The day of their use, the culture medium was changed to a standard physiological medium, similar to that used for DRG neurons (see paragraph 2.4), for a minimum of 15 min at 37°C prior to experiments. The cells plated on coverslips were then transferred in the recording bath filled with the standard physiological medium. For automated patch-clamp recordings, the day of their use, the cells were transferred in Eppendorf tubes containing a FreeStyle 293 expression medium (Gibco; #12338) which were then placed in the automated electrophysiology platform.

2.6. Electrophysiological recordings from the mouse neuromuscular system in vivo

Recordings from the neuromuscular system of anaesthetized mouse were obtained by means of a minimally-invasive electrophysiological method, using the Qtrac© software (Prof. H. Bostock, Institute of Neurology, London, United Kingdom), as previously detailed (Marrouchi et al., 2013). Briefly, the anaesthetized mice were placed on a heating pad to maintain body temperature throughout the experiments (between 35.94 ± 0.05 and 35.99 ± 0.03°C, as determined in 29 mice using a rectal probe). Electrical stimulations were delivered to the caudal motor nerve (at the base of the tail) by surface electrodes, and the compound muscle action potential (CMAP)

was recorded using needle-electrodes inserted into the tail muscle. To study the local action of HwTx-IV and TTX, intramuscular (i.m.) injections (4-µL maximal volume) of PBS 1X solution containing various concentrations of a given toxin were delivered with a 10-µL micro-syringe at the base of mouse tail, between stimulation and ground electrodes. Similar injections (4 µL) were also done with PBS 1X solution to test an eventual effect of the vehicle.

On-line recordings were initiated approximatively 5 min before a given injection to determine the toxin and/or vehicle effects on selected excitability parameters, such as the excitability threshold and CMAP amplitude continuously registered as a function of time. To better identify the underlying mechanism(s) of action and the duration of HwTx-IV and TTX effects, five different excitability tests (stimulus-response, strength-duration and current-threshold relationships, as well as threshold electrotonus and recovery cycle; detailed in Cerles et al., 2017) were performed together before and at various times (from ~30 min to ~12 h) after a given injection. As a whole, more than thirty parameters were determined from these five excitability tests, and analyzed. Most of them provide specific and complementary information on the density and functional status of ion channels, receptors and pumps, as well as on the passive membrane properties of the neuromuscular system (Kiernan and Bostock, 2000; Krishnan et al., 2008).

2.7. Mechanical recordings from isolated mouse neuromuscular preparations

Measurements of isometric contractile force (*i.e.* single twitch), elicited by stimulating the muscle either indirectly *via* the phrenic nerve or directly, were performed as previously described (Schlumberger et al., 2010). Briefly, the central tendon of the hemidiaphragm was attached to an isometric force displacement transducer (FT03 model; Grass Instruments, West Warwick, RI, USA) *via* an adjustable stainless-steel hook, and the other tendon (at the rib side) was securely anchored onto the silicone-coated bath. A mobile micrometer stage allowed adjusting the muscle length to obtain maximal contractile responses. The resting tension was monitored and kept constant throughout the experiment.

Electrical square pulses of 200 µs duration and supramaximal voltage (15-20 V for nerve stimulation and 80-100 V for direct stimulation) were delivered by a stimulator (S-48 model; Grass Instruments) at a frequency of 0.1 Hz. Signals from

the force transducer were amplified, collected, and digitized with the aid of a computer equipped with an analog-to-digital converter (Digidata-1322A model; Molecular Devices, Sunnyvale, CA, USA) managed by the Axoscope 9.2 software (Molecular Devices). The collected signals were analyzed off-line using the Clampfit 9.2 program (Molecular Devices). The experiments were carried out at constant room temperature (22°C).

2.8. Automated patch-clamp recordings from HEK-293 and CHO cells

Whole-cell automated patch-clamp experiments were performed on a QPatch HTX automated electrophysiology platform (Sophion Bioscience, Ballerup, Denmark), allowing both signal acquisition and data analyses (Bell and Dallas, 2017). The extracellular medium composition of hNa_V-overexpressing HEK293 cells was (in mM): NaCl 154, KCl 4, $CaCl_2$ 2, $MgCl_2$ 1, and HEPES 10 (pH 7.4, adjusted with NaOH), and that of intracellular (*i.e.* path-clamp pipette) medium: CsF 150, EGTA/CsOH 1/50, HEPES 10, NaCl 10, $MgCl_2$ 1, and $CaCl_2$ 1 (pH 7.4, adjusted with CsOH). The extracellular medium composition of $hCa_V1.2$-overexpressing CHO cells was (in mM): NaCl 145, KCl 4, $CaCl_2$ 10, and HEPES 10 (pH 7.4, adjusted with NaOH), and that of intracellular medium: CsF 27, CsCl 112, EGTA 8.2, HEPES 10, NaCl 2, and Mg-ATP 4 (pH 7.4, adjusted with CsOH). The extracellular medium composition of $hK_V11.1$-overexpressing CHO cells was (in mM): NaCl 145, KCl 4, $CaCl_2$ 2, $MgCl_2$ 1, HEPES 10, and D-glucose 10 (pH 7.4, adjusted with NaOH), and that of intracellular medium: KCl 120, $CaCl_2$ 5.4, EGTA 10, HEPES 10, Mg-ATP 4, and $MgCl_2$ 1.75 (pH 7.4, adjusted with KOH). HwTx-IV was diluted in the extracellular medium added with bovine serum albumin (0.1%), to give the final concentrations indicated in the text. The times of incubation varied between ~2 and ~7 min to achieve steady-state effects. The experiments were carried out at room temperature (20-22°C).

The hNa_V-overexpressing HEK-293 cells were maintained at a holding potential of either -90 mV ($hNa_V1.5$) or -100 mV (other hNa_V channel subtypes). Currents were elicited at a frequency of 0.2 Hz by 20-ms test-pulses to -20 mV ($hNa_V1.1$, 1.2, 1.4, and 1.7), -10 mV ($hNa_V1.3$), -40 mV ($hNa_V1.5$), -15 mV ($hNa_V1.6$) or +10 mV ($hNa_V1.8$), preceded by 200-ms ($hNa_V1.5$) or 40-ms ($hNa_V1.7$) pulses to -120 mV, or not ($hNa_V1.1$, 1.2, 1.3, 1.4 and 1.6). The $hCa_V1.2$-overexpressing CHO

cells were maintained at a holding potential of -50 mV, and currents were elicited at a frequency of 0.05 Hz by 200-ms test-pulses to +0 mV. The hK_V11.1-overexpressing CHO cells were maintained at a holding potential of -80 mV, and tail currents were elicited at a frequency of 0.07 Hz by 5-s test-pulses to -50 mV, preceded by 4.8-s pulses to +20 mV following 20-ms pulses to -50 mV. The concentration-response relationships were established by expressing the peak amplitude of the sum of ten cell currents recorded in the presence of a given HwTx-IV concentration relatively to that of the sum of these currents recorded before toxin incubation.

2.9. Manual patch-clamp recordings from HEK-293 cells and mouse DRG neurons

Whole-cell manual patch-clamp experiments were performed by using a MultiClamp 700B integrating patch-clamp amplifier and the pClamp10.6 software (Molecular Devices, Sunnyvale, CA, USA), as previously described (Schlumberger et al., 2014). The signals, acquired at a 4-kHz sample rate, were filtered at 2 kHz with a low-pass Bessel filter and digitized with the aid of a computer equipped with an analog-to-digital converter (Digidata-1440A model; Molecular Devices). The patch-clamp pipettes were filled with a medium composed of (in mM): CsCl 90, $CsMeSO_3$ 40, NaCl 10, $MgCl_2$ 2, EGTA 2, ATP-Na_2 4, and HEPES 10 (pH 7.32, adjusted with CsOH), and had ~3-MΩ resistance in the standard physiological medium. A fast perfusion system allowed changing the solution (standard physiological medium added or not with a given toxin concentration) around the recorded cell within a few seconds. The experiments were carried out at constant room temperature (22°C).

The cells were maintained at a holding potential of -60 mV, and currents were elicited at a frequency of 0.5 Hz by 50-ms test-pulses to -20 mV (+10 mV for hNa_V1.6-overexpressing HEK-293 cells) preceded by 1-s pulses to -120 mV. The concentration-response relationships were established by expressing the peak current amplitude measured in the presence of a given toxin concentration relatively to that before toxin application. Current-voltage relationships were obtained by varying test-pulses from -80 to +10 mV in 5-mV increments, and steady-state inactivation-voltage relationships by changing pre-pulses from -120 to -20 mV in 5-mV increments.

2.10. Data and statistical analyses

Concentration-response relationships were established by plotting the response, recorded in the presence of a given toxin (Rt) and expressed as percentage of the value obtained in absence of toxin (Rc), against the toxin concentration ([toxin]). The theoretical concentration-response curves were calculated from typical sigmoid nonlinear regressions through data points (correlation coefficient = r^2) according to the Hill equation (GraphPad Prism 5 or QPatch assay software): $Rt / Rc = 1 / [1 + ([toxin] / IC_{50}) n_H]$, where n_H is the Hill number.

Conductance (g) was calculated according to the following equation: $g = I / (V_T – V_{Na})$, where I is the peak current amplitude, V_T is the test-pulse voltage, and V_{Na} is the equilibrium potential of Na ions. Conductance-voltage relationships were established by plotting the conductance, expressed as percentage of the maximal conductance (gmax) calculated at large positive test-pulses, as a function of test-pulse voltage. The theoretical curves correspond to data point fits, according to the Boltzmann equation (GraphPad Prism 5 software): $g / gmax = 1 – [1 / (1 + \exp ((V_T – V_{T50\%}) / k_g))]$, where $V_{T50\%}$ is the test-pulse voltage corresponding to 50% maximal conductance, and k_g is the slope of the curve.

Steady-state inactivation-voltage relationships were established by plotting the peak current amplitude, expressed as percentage of the maximal amplitude (Imax) recorded in response to large negative pre-pulses, as a function of pre-pulse voltage (V_P). The theoretical curves correspond to data point fits, according to the Boltzmann equation (GraphPad Prism 5 software): $I / Imax = 1 / [1 + \exp ((V_P – V_{P50\%}) / k_h)]$, where $V_{P50\%}$ is the pre-pulse voltage corresponding to 50% maximal peak amplitude of current, and k_h is the slope of the curve.

Current kinetics were evaluated by calculating the two following activation and inactivation parameters: (1) the time to peak (tp), defined as the time between test-pulse triggering and the peak current, and (2) the time constant (τh) of the current decay, assuming that the current inactivation is a mono-exponential decay as a function of time, *i.e.* $I_{(t)} = I_{(0)} e^{(-t/\tau h)}$.

Data are expressed as means ± standard deviations (S.D.) of n different experiments. The statistical comparison of values was carried out using the parametric two-tailed Student's *t*-test (either paired samples for comparison within a single population or unpaired samples for comparison between two populations), the 2-factor ANOVA test or the nonparametric Mann-Whitney U test, according to the

equality of sample variances estimated with the Lilliefors test. Differences between values were considered to be statistically significant at $P \leq 0.05$.

3. Results

3.1. Effects of HwTx-IV and TTX on the mouse neuromuscular system in vivo

On-line recordings revealed that the major effect of i.m. injections of PBS 1X solutions containing various concentrations of either HwTx-IV (from 4.1 pmol/kg to 41.4 nmol/kg mouse) or TTX (from 3.4 pmol/kg to 166.5 nmol/kg mouse) to anaesthetized mice was a marked concentration-dependent decrease of CMAP amplitude. This is exemplified in Fig. 1A (insets) for CMAP recordings performed before and ~10 min after injections of 41.4 nmol HwTx-IV and 166.5 nmol TTX per kg of mouse. This effect occurred within various times, depending on the concentration of toxin injected, ranging from ~10 to ~20 min (Fig. 1A). It is worth noting that the maximal CMAP amplitude remained stable before toxin injections and during ~25 min after injection of 3.4 pmol/kg mouse of TTX. Moreover, the maximal CMAP amplitude measured ~30 min after injections of PBS 1X solution alone, and compared to values before injections, was not significantly affected, *i.e.* 97.8 ± 2.3% (n = 8 mice), indicating (i) that injections of the toxin vehicle had no effect on the maximal CMAP amplitude and (ii) that no marked run-down of the response occurred.

The toxin blocking effect was quantified by establishing the concentration-response curves, *i.e.* the maximal CMAP amplitude as a function of the concentration of toxin injected, and determining the IC_{50} values (see for more details the Material and methods section). As shown in Fig. 1B, the concentration-response curves for HwTx-IV and TTX revealed IC_{50} values of 0.9 and 1.9 nmol/kg mouse, respectively. It thus appears that HwTx-IV was approximatively 2 times more efficient than TTX, on equimolar basis, to inhibit the CMAP.

Figure 1 near here

The five different excitability tests (stimulus-response, strength-duration and current-threshold relationships, as well as threshold electrotonus and recovery cycle) were performed together before and ~30 min after i.m. injections of PBS 1X solution containing HwTx-IV (4.1-41.4 nmol/kg mouse) or TTX (5.3-17.8 nmol/kg mouse), and the derived neuromuscular excitability parameters were determined (Supplementary

data, Fig. S1, Fig. S2 and Table S1). With the exception of decreased maximal CMAP amplitude and increased stimulus intensity required to generate a 50% maximal amplitude CMAP (stimulus-response relationship; Fig.S1Aa, Fig. S2Aa and Table S1), analysis of strength-duration relationship, threshold electrotonus, current-threshold relationship, and recovery cycle did not reveal other HwTx-IV and TTX effects since no significant modification of excitability waveforms and derived parameters was detected (Fig. S1B-E, Fig. S2B-E and Table S1). The toxin-induced effects were completely reversed within ~12 h after HwTx-IV (4.1-41.4 nmol/kg mouse) or TTX (5.3-17.8 nmol/kg mouse) injections (Fig. S3 and Table S1).

It should be emphasized that injections of 41.4 and 394.3 nmol HwTx-IV per kg of mouse (concentrations corresponding to 46 and 438 times the IC_{50} value, respectively) caused death of 40% (2/5) and 80% (4/5) of the mice, respectively, within one hour. Similarly, injections of 17.8 and 166.5 nmol TTX per kg of mouse (*i.e.* 9 and 88 times the IC_{50} value, respectively) produced death of 43% (3/7) and 75% (6/8) of the animals, respectively, within one hour. These results indicate a more than 2-time lower *in vivo* toxicity of HwTx-IV compared to TTX.

3.2. Effects of HwTx-IV on isolated mouse neuromuscular preparations

The evaluation of HwTx-IV effects on isolated mouse phrenic nerve-hemidiaphragm preparations revealed that various toxin concentrations (from 152 nM to 14 µM) produced an inhibition of both nerve-evoked and directly-elicited muscle contractile force of single twitches. This is illustrated in Fig. 2A (insets) for twitch recordings performed in the absence and in the presence of 14 µM HwTx-IV. The toxin-induced blockade of nerve-evoked muscle twitch was concentration- and time-dependent (Fig. 2). In particular, a complete inhibition of nerve-evoked contractile response occurred within ~8 min after addition of 14 µM HwTx-IV to the standard physiological medium, as exemplified by the representative time-course of toxin effect shown in Fig. 2A.

Figure 2 near here

Similarly, the toxin (14 µM) produced a marked decrease of directly-elicited muscle twitch within ~8 min (Fig. 2A). However, the maximal amplitude of directly-elicited muscle twitch was much less affected by HwTx-IV concentrations from 152 nM to 14 µM than the nerve-evoked twitch. In particular, when muscle twitch evoked

by nerve stimulation was completely blocked by 14 µM HwTx-IV (*i.e.* maximal amplitude reduced to 1.2 ± 0.9% of initial values measured in the absence of toxin, n = 5 muscles), a contractile response, although of low maximal amplitude (*i.e.* 16.9 ± 1.3% of initial values measured in the absence of toxin, n = 5 muscles), could be still obtained by direct stimulation of hemidiaphragms. For comparison, an only slightly higher maximal amplitude (*i.e.* 24.2 ± 2.6% of initial values measured in the absence of toxin, n = 10 muscles) was obtained when muscle twitch was evoked by nerve stimulation in the presence of 152 nM HwTx-IV (Fig. 2B). It is worth noting that no decrease of twitch amplitude occurred when neuromuscular preparations were only bathed with standard physiological medium for 20 min (data not shown). This indicates, in particular, that there was no important run-down of twitch amplitude under these experimental conditions.

Assuming that n_H was equal to 1, IC_{50} values of 30 and 900 nM were calculated according to the Hill equation (see Material and methods section for more details), for the toxin-induced decrease of maximal amplitude of nerve-evoked and directly-elicited muscle twitches, respectively. HwTx-IV was therefore 30 times more efficient to inhibit nerve-evoked than directly-elicited muscle contractile force of isolated mouse hemidiaphragms.

3.3. Effects of HwTx-IV and TTX on hNa$_V$1.1-1.8-overexpressing HEK-293 cells and on CHO cells overexpressing hCav1.2 and hKv11.1 channel subtypes

Whole-cell automated patch-clamp experiments performed on HEK-293 cells overexpressing hNa$_V$1.1-1.8 channel subtypes revealed the following increasing order for IC_{50} values obtained from the concentration-response curves of HwTx-IV effects on currents flowing through the different channel subtypes (Fig. 3): hNa$_V$1.1 (41 ± 1 nM, n = 4) > hNa$_V$1.2 (44 ± 2 nM, n = 10) > hNa$_V$1.6 (52 ± 9 nM, n = 3) > hNa$_V$1.7 (100 ± 6 nM, n = 4) > hNa$_V$1.3 (190 ± 24 nM, n = 7) > hNa$_V$1.4 (> 10 µM, n = 8) for TTX-S (IC_{50} values between 3 ± 2 and 78 ± 2 nM, n = 2-5) channel subtypes, and hNa$_V$1.5 = hNa$_V$1.8 (> 10 µM, n = 7-9) for TTX-resistant (TTX-R; IC_{50} values of 3 ± 1 and > 10 µM, respectively, n = 5) channel subtypes. Therefore, all the TTX-R channel subtypes studied were also relatively resistant to HwTx-IV while all the TTX-S channel subtypes studied, with the exception of hNa$_V$1.4 channel subtype, were also relatively sensitive to HwTx-IV. Additionally, HwTx-IV was ~2 times more potent

to block $hNa_V1.6$ than $hNa_V1.7$ channel subtypes. It is worth noting that the toxin had very low affinity for $hCa_V1.2$ and $hK_V11.1$ channel subtypes overexpressed in CHO cells since the IC_{50} values obtained from the concentration-response curves of HwTx-IV effects on currents flowing through these two ion channels were higher than 10 µM (n = 2-4, data not shown).

Figure 3 near here

Detailed experiments, using whole-cell manual patch-clamp, displayed IC_{50} values of 83.3 and 32.6 nM from the concentration-response curves of HwTx-IV effects on currents flowing through $hNa_V1.6$ and $hNa_V1.7$ channel subtypes overexpressed in HEK-293 cells, respectively (Fig. 4A). Under these conditions, the toxin was thus approximatively 2.5 times less efficient to block $hNa_V1.6$ than $hNa_V1.7$ channel subtypes. This HwTx-IV-induced blocking action occurred without any change in steady-state inactivation- and conductance-voltage relationships of $hNa_V1.6$ and $hNa_V1.7$ channel subtypes, as shown in Fig. 4B-C and Table 1 for toxin concentrations of 70-100 and 20 nM, respectively, *i.e.* close to the IC_{50} values.

Figure 4 and Table 1 near here

3.4. Effects of HwTx-IV and TTX on mouse DRG neurons

Before evaluating the effects of HwTx-IV on the sodium currents of DRG neurons, the TTX sensitivity of these currents was first determined by perfusion of cells with a standard physiological medium containing 100 nM TTX. Under this condition, two types of neurons were recorded (Fig. 5A): those (67%, *i.e.* 12/18 cells) having TTX-S current, *i.e.* which was blocked by the toxin to 5 ± 5% of initial peak amplitude values within 1 min, and those (33%, *i.e.* 6/18 cells) having TTX-R current, *i.e.* which was blocked by the toxin, perfused for ~6 min, to 83 ± 6% of initial peak amplitude values but was completely inhibited by 100 µM TTX. It should be noted that the activation and inactivation kinetics of TTX-R current were significantly slower than those of TTX-S current (Fig. 5A and Table 2).

Table 2 near here

After washing-out TTX by perfusion of neurons with a toxin-free solution for 8-10 min, the cell perfusion with standard physiological solutions containing various HwTx-IV concentrations (from 5 nM to 20 µM) produced then a decrease of sodium current amplitude which was dependent on the time following the perfusion, the toxin

concentration and the current sensitivity to TTX. In particular, the concentration-response curves of HwTx-IV effects on the peak amplitude of TTX-S and TTX-R currents revealed IC_{50} values of 0.13 and 110 µM, respectively (Fig. 5B). It thus appears that the toxin was approximatively 850 times more efficient to inhibit TTX-S than TTX-R sodium currents of mouse DRG neurons. The blocking effects of HwTx-IV on the peak amplitude of TTX-S current were stationary approximatively 7 and 2 min after perfusion of 0.005 and 1 µM of toxin, respectively. Those on the peak amplitude of TTX-R current were stationary approximatively 6 min after perfusion of 10 to 20 µM of toxin. The HwTx-IV effects on TTX-R current, not very noticeable, were not further studied, in contrast to those on TTX-S current.

Figure 5 near here

The peak amplitude of TTX-S current, which was 9 and 3% of initial values after perfusion of 1 and 10 µM HwTx-IV, respectively, returned to 43 ± 17% of initial values (n = 9) by perfusion of neurons with a toxin-free solution for 15-20 min. The analyses of activation and inactivation kinetics of TTX-S sodium current in the absence and in the presence of HwTx-IV concentrations close to the IC_{50} value (*i.e.* 0.1 µM) revealed that the toxin did not affect these kinetics since tp and τh were not significantly modified (Table 2). Similarly, HwTx-IV (0.1 µM) did not produce any alteration of steady-state inactivation- and conductance-voltage relationships for neurons exhibiting TTX-S current (Fig. 5C and Table 1).

4. Discussion

The present study was undertaken to determine the interaction between HwTx-IV and $Na_V1.6$ channel subtype, using multiscale (from *in vivo* to individual cell) functional approaches. The results obtained can be summarized as follow: (i) HwTx-IV was approximatively 2 times more efficient than TTX to inhibit the CMAP recorded from the mouse skeletal neuromuscular system *in vivo*, (ii) HwTx-IV was approximatively 30 times more effective to inhibit nerve-evoked than directly-elicited muscle contractile force in isolated mouse hemidiaphragms, (iii) HwTx-IV was more potent to block TTX-S ($hNa_V1.1$, 1.2, 1.3, 1.6 and 1.7, with the exception of $hNa_V1.4$) than TTX-R ($hNa_V1.5$ and 1.8) Na_V channel subtypes overexpressed in HEK-293 cells, (iv) HwTx-IV was approximatively 850 times more efficient to inhibit TTX-S than

TTX-R sodium currents of mouse DRG neurons, and (v) the *in vivo* toxicity of HwTx-IV was more than 2 times lower than that of TTX.

The effects of i.m. injections of HwTx-IV and TTX on the mouse neuromuscular system *in vivo* consisted in an inhibition of CMAP and an increase in the stimulus intensity required to generate a 50% maximal amplitude CMAP. The duration of the observed effects was less than 12 h. These results strongly suggest that HwTx-IV and TTX produce a marked and reversible decrease of sodium currents, *i.e.* of the density and/or functional status of "transient" Na_V channels, as might be expected with toxins known to block these types of channels (Cestèle and Catterall, 2000). Besides these effects, HwTx-IV and TTX did not modify other excitability parameters, indicating that the two toxins do not affect the density and functional status of other types and subtypes of ion channels, receptors and pumps, nor the passive membrane properties of the neuromuscular system (Kiernan and Bostock, 2000; Krishnan et al., 2008).

The HwTx-IV-induced inhibition of CMAP could be explained by an *in vivo* action of this toxin on the Na_V channel subtypes identified so far in adult nerves and skeletal muscles, *i.e.* the $Na_V1.6$ and $Na_V1.4$ channel subtypes, respectively (Caldwell et al., 2000; de Lera Ruiz and Kraus, 2015). HwTx-IV would be approximatively 2 times more efficient than TTX to interact with and to block $Na_V1.6$ and/or $Na_V1.4$ channel subtypes. Available *in vitro* evidence indicated however that the $Na_V1.4$ channel subtype is not preferentially sensitive to HwTx-IV since the toxin affinity for this channel subtype (IC_{50} > 10 µM; Xiao et al., 2008) was more than 1000 times less than that of TTX (IC_{50} ≈ 8 nM; Tsukamoto et al., 2017), without giving information on the interaction between HwTx-IV and $Na_V1.6$ channel subtype. It was therefore probable that the relative high efficiency of HwTx-IV to inhibit *in vivo* the CMAP, compared to TTX, results from toxin-induced preferential blockade of the $Na_V1.6$ and not $Na_V1.4$ channel subtype. This hypothesis was tested directly by studying the HwTx-IV effects on isolated mouse neuromuscular preparations and recording the isometric contractile force elicited by stimulating either directly the muscle or indirectly *via* its associated motor nerve.

The study of HwTx-IV effects on isolated mouse phrenic nerve-hemidiaphragm preparations reveals that the toxin produced an inhibition of the nerve-evoked contractile force with a calculated IC_{50} value of 30 nM. These results confirm those

obtained *in vivo* on the CMAP recorded from tail muscle in response to caudal motor nerve stimulation, *i.e.* the relative high affinity of HwTx-IV for $Na_V1.6$ and/or $Na_V1.4$ channel subtypes. It is worth noting that HwTx-IV was previously reported to completely block the conduction of isolated mouse phrenic nerve-hemidiaphragm preparations, by acting on multiple ion channel proteins, especially the Ca_V channels (Yu et al., 2014). However, this is not supported by the present results showing a very low affinity of the peptide for $hCa_V1.2$ channel subtype overexpressed in CHO cells.

Additionally, HwTx-IV also inhibited the directly-elicited muscle twitch of isolated mouse hemidiaphragms with a calculated IC_{50} value of 300 nM. The conditions of direct muscle stimulation are very interesting because it makes possible to decrease the implication of $Na_V1.6$ channel subtype (located in nerves and not in muscles; Caldwell et al., 2000) in the contractile response, and thus to get direct information on the affinity of interaction between HwTx-IV and $Na_V1.4$ channel subtype (located in skeletal muscles and not in nerves; de Lera Ruiz and Kraus, 2015). The results obtained under these conditions therefore strongly suggest that the toxin was 30 times less potent to block the $Na_V1.4$ than the $Na_V1.6$ channel subtype. These results confirm the hypothesis that the HwTx-IV-induced inhibition of nerve-evoked hemidiaphragm twitch and of the CMAP recorded *in vivo* from tail muscle in response to caudal motor nerve stimulation resulted from a preferential blockade of $Na_V1.6$ channel subtype by the toxin.

The following step was thus to undertake the study of HwTx-IV effects on HEK-293 cells overexpressing $hNa_V1.1$-1.8 channel subtypes to get complementary information on the relative selectivity of interaction between the toxin and $Na_V1.6$ channel subtype, as well as on the relative IC_{50} value of HwTx-IV on this channel subtype, since poor evidence was available in the literature (Rahnama et al., 2017).

The results obtained from whole-cell automated patch-clamp experiments performed on HEK-293 cells overexpressing $hNa_V1.1$-1.8 channel subtypes highlighted two groups of channel subtypes: (i) a relatively HwTx-IV-sensitive group (IC_{50} = 41-190 nM) including, by increasing order of IC_{50} values, $hNa_V1.1$ > $hNa_V1.2$ > $hNa_V1.6$ > $hNa_V1.7$ > $hNa_V1.3$, and (ii) a relatively HwTx-IV-resistant group (IC_{50} > 10 µM) composed of $hNa_V1.4$ ≈ $hNa_V1.5$ ≈ $hNa_V1.8$. These results are similar to the following sequence of peptide affinities reported so far in the literature, with respect

552 to the Na_V channel subtype overexpressed in HEK-293 cells: $hNa_V1.7$ (IC_{50} = 26 nM)
553 > $rNa_V1.2$ (IC_{50} = 150 nM) > $rNa_V1.3$ (IC_{50} = 338 nM) >> $rNa_V1.4$ ≈ $hNa_V1.5$ (IC_{50} > 10
554 µM) (Xiao et al., 2008). The slight IC_{50} differences between the two studies may
555 reflect those between the species, human or rat (r), of the Na_V channel subtypes
556 studied. It seems therefore that the selectivity of HwTx-IV towards $hNa_V1.7$ is not as
557 important as previously reported since the toxin is also highly potent to block
558 $hNa_V1.1$, $h(r)Na_V1.2$, $h(r)Na_V1.3$ and $hNa_V1.6$ channel subtypes. However, the
559 discovery that $Na_V1.1$ and 1.3 channel subtypes are involved in pain pathways (Chen
560 et al., 2014; Osteen et al., 2016; Cardoso and Lewis, 2017) and that $Na_V1.2$ channel
561 subtype is only located in the central nervous system (see de Lera Ruiz and Kraus,
562 2015) does not impair further development of HwTx-IV as a potential antinociceptive
563 agent to access only peripheral Na_V channel subtypes. In contrast, the fact that this
564 toxin also targets $Na_V1.6$ channel subtype is more problematic because of the
565 resulting side-effects which limit its *in vivo* efficacy in pre-clinical pain models.

566 The poor selectivity of HwTx-IV for $hNa_V1.7$ over $hNa_V1.6$ channel subtypes is
567 further supported by the recent characterization of the effects of a triple-mutant of
568 HwTx-IV (E1G, E4G and Y33W; m3-HwTx-IV) on either HEK-293 cells
569 overexpressing $hNa_V1.1$-1.5 channel subtypes, and the β1 auxiliary subunit, or CHO
570 cells overexpressing $hNa_V1.6$-1.7 and $hNa_V1.8$/β3 channel subtypes (Rahnama et al.,
571 2017). Despite the fact that mutations may influence the peptide selectivity over Na_V
572 channel subtypes, this study revealed quite similar Na_V channel subtype selectivity,
573 but higher blockade potency of the recombinant peptide, compared to HwTx-IV
574 (present results): $hNa_V1.7$ > $hNa_V1.6$ > $hNa_V1.3$ > $hNa_V1.1$ > $hNa_V1.2$ (IC_{50} = 3.3-
575 11.9 nM) >> $hNa_V1.4$ (IC_{50} = 369 nM) >>> $hNa_V1.5$ ≈ $hNa_V1.8$ (IC_{50} > 1 µM). Taken
576 altogether, these data indicate that all the TTX-R channel subtypes studied (TTX IC_{50}
577 = 3-10 µM) were also resistant to HwTx-IV and m3-HwTx-IV blockade, while all the
578 TTX-S channel subtypes studied (TTX IC_{50} = 3-78 nM), with the exception of $hNa_V1.4$
579 channel subtype, were also sensitive to HwTx-IV and m3-HwTx-IV inhibition.

580 The effects of HwTx-IV were further investigated on TTX-S and TTX-R Na_V
581 channel subtypes of adult mouse DRG neurons, *i.e.* mainly the TTX-S $Na_V1.1$, 1.6
582 and 1.7 channel subtypes and the TTX-R $Na_V1.8$ and 1.9 channel subtypes (Rush et
583 al., 2007). This study was motivated, on one hand, by the well-known important role
584 of DRG neurons as the primary sensitive pathway of chronic pain and, on the other

hand, by the absence of report of such study in mouse, until now. The effects consisted in a marked and reversible decrease of the peak amplitude of TTX-S sodium current (IC_{50} = 0.13 µM), without any significant modification of activation and inactivation kinetics and voltage-dependencies. As expected from the results obtained from whole-cell automated patch-clamp experiments, the peptide was approximatively 850 times less efficient in inhibiting the peak amplitude of TTX-R sodium current (IC_{50} = 110 µM). From this point of view, HwTx-IV is very interesting compared to TTX which was only approximately 90 times more potent to block TTX-S than TTX-R Na_V channel subtypes (IC_{50} values of 5.5 and 500 nM, respectively).

These results are consistent with previous observations on adult rat DRG neurons showing that 0.1 µM HwTx-IV inhibited TTX-S sodium current, without any alteration of activation and inactivation kinetics, but had no effect on TTX-R currents (Peng et al., 2002). Interestingly, the activation and inactivation kinetics of TTX-R sodium current were slower than those of TTX-S sodium current. This is due to the prevalence of TTX-R $Na_V1.8$ and to a less extent of $Na_V1.9$ channel subtypes which are exceptionally characterized by slow ($Na_V1.8$) and even very slow ($Na_V1.9$) activation and inactivation kinetics (Rush et al., 2007).

During experiments aimed to study the effects of i.m. injections of HwTx-IV and TTX on the mouse neuromuscular system *in vivo*, 17.8 and 166.5 nmol TTX per kg of mouse (corresponding to 9 and 88 times the *in vivo* IC_{50} value, respectively) produced death of 43% and 75% of the animals, respectively, within one hour. These values are close to those reported in the literature, *i.e.* i.m. injections of 5.3 µg (16.6 nmol) TTX per kg rodent caused the death of 50% of the animals (Xu et al., 2003). By comparison, i.m. injections of HwTx-IV concentrations corresponding to 46 and 438 times the *in vivo* IC_{50} value produced death of 40% and 80% of the mice, respectively, within one hour. Although these results indicate a more than 2-time lower *in vivo* toxicity of HwTx-IV compared to TTX, the resulting side-effects of the peptide may limit its use as a potential lead molecule for the development of novel pain therapeutics. In particular, the therapeutic window of HwTx-IV as an analgesic appears to be markedly reduced taking into account that the peptide was previously reported to have analgesic activity at 100 µg/kg mouse (*i.e.* 24 nmol/kg mouse) when i.m. injected to animals (Liu et al., 2014a).

Since HwTx-IV had very low affinity for $hNa_V1.5$ channel subtype, as well as

for $hCa_V1.2$ and $hK_V11.1$ channel (IC_{50} > 10 µM), it is unlikely that the death of mice resulted from heart dysfunctioning. In contrast, given the poor selectivity of the peptide over $Na_V1.6$ channel subtype, it is likely that impaired motor functioning is involved since peptides interacting with this subtype of Na_V channels are well-known to typically lead to such severe side-effects.

5. Conclusion

To the best of our knowledge, this is the first report showing directly that high affinity interaction occurs between HwTx-IV and $Na_V1.6$ channel subtype. Indeed, the toxin has been reported so far in the literature as being highly specific for the $Na_V1.7$ channel subtype, without effects on the $Na_V1.6$ channel subtype being evidenced. The present study showing quite similar affinities of HwTx-IV for $Na_V1.6$ and $Na_V1.7$ channel subtypes allows better understanding the mechanisms of motor *in vivo* side-effects produced by this peptide, and makes this molecule significantly less attractive for an eventual therapeutic use as antinociceptive agent.

Acknowledgments

This research was funded by a collaborative grant (#153114) between Sanofi-Aventis Research & Development (Chilly-Mazarin, France) and the French Alternative Energies and Atomic Energy Commission (CEA, Gif-sur-Yvette, France). T.C.G. was supported by a doctoral CIFRE fellowship from Sanofi-Aventis. The authors are grateful to thank Dr Andrees Bohme and Brigitte Schombert for their help in the establishment of $hCa_V1.2$ and $hK_V11.1$ electrophysiological protocols, and Sophie Fontaine for her technical assistance for the Na_V cell lines management.

Conflict of interest

The authors declare that they have no actual or potential conflict of interest including any financial, personal or other relationships with other people or organizations within three years of beginning this work.

References

Bell D.C., Dallas M.L., 2017. Using automated patch clamp electrophysiology platforms in pain-related ion channel research: insights from industry and academia. Br. J. Pharmacol. *in press*. doi: 10.1111/bph.13916.

Caldwell J.H., Schaller K.L., Lasher R.S., Peles E., Levinson S.R., 2000. Sodium channel Na(v)1.6 is localized at nodes of Ranvier, dendrites, and synapses. Proc. Natl Acad. Sci. USA. 97, 5616-5620.

Cardoso F.C., Lewis R.J., 2017. Sodium channels and pain: from toxins to therapies. Br. J. Pharmacol. *in press*. doi: 10.1111/bph.13962.

Catterall W.A., 2000. From ionic currents to molecular mechanisms: the structure and function of voltage-gated sodium channels. Neuron 26, 13-25.

Cerles O., Benoit E., Chéreau C., Chouzenoux S., Morin F., Guillaumot M.A., Coriat R., Kavian N., Loussier T., Santulli P., Marcellin L., Saidu N.E., Weill B., Batteux F., Nicco C., 2017. Niclosamide inhibits oxaliplatin neurotoxicity while improving colorectal cancer therapeutic response. Mol. Cancer Ther. 16, 300-311.

Cestèle S., Catterall W.A., 2000. Molecular mechanisms of neurotoxin action on voltage-gated sodium channels. Biochimie 82, 883-892.

Chen H.P., Zhou W., Kang L.M., Yan H., Zhang L., Xu B.H., Cai W.H., 2014. Intrathecal miR-96 inhibits NaV1.3 expression and alleviates neuropathic pain in rat following chronic construction injury. Neurochem. Res. 39, 76-83.

de Lera Ruiz M., Kraus R.L., 2015. Voltage-gated sodium channels: Structure, function, pharmacology, and clinical indications. J. Med. Chem. 58, 7093-7118.

Deuis J.R., Wingerd J.S., Winter Z., Durek T., Dekan Z., Sousa S.R., Zimmermann K., Hoffmann T., Weidner C., Nassar M.A., Alewood P.F., Lewis R.J., Vetter I., 2016. Analgesic effects of GpTx-1, PF-04856264 and CNV1014802 in a mouse model of NaV1.7-mediated pain. Toxins (Basel) 8, pii: E78.

Flinspach M., Xu Q., Piekarz A.D., Fellows R., Hagan R., Gibbs A., Liu Y., Neff R.A., Freedman J., Eckert W.A., Zhou M., Bonesteel R., Pennington M.W., Eddinger K.A., Yaksh T.L., Hunter M., Swanson R.V., Wickenden A.D., 2017. Insensitivity to pain induced by a potent selective closed-state Nav1.7 inhibitor. Sci Rep. 7, 39662.

Goldin A.L., Barchi R.L., Caldwell J.H., Hofmann F., Howe J.R., Hunter J.C., Kallen

R.G., Mandel G., Meisler M.H., Netter Y.B., Noda M., Tamkun M.M., Waxman S.G., Wood J.N., Catterall W.A., 2000. Nomenclature of voltage-gated sodium channels. Neuron 28, 365-368.

Kiernan M.C., Bostock H., 2000. Effects of membrane polarization and ischaemia on the excitability properties of human motor axons. Brain 123, 2542-2551.

Klint J.K., Senff S., Rupasinghe D.B., Er S.Y., Herzig V., Nicholson G.M., King G.F., 2012. Spider-venom peptides that target voltage-gated sodium channels: pharmacological tools and potential therapeutic leads. Toxicon 60, 478-491.

Krishnan A., Park S., Lin C.S., Kiernan M.C., 2008. Assessment of nerve excitability in toxic and metabolic neuropathies. J. Peripher. Nerv. Syst. 13, 7-26.

Liu Y., Wu Z., Tang D., Xun X., Liu L., Li X., Nie D., Xiang Y., Yi J., Yi J., 2014a. Analgesic effects of huwentoxin-IV on animal models of inflammatory and neuropathic pain. Protein Pept Lett. 21, 153-158.

Liu Y., Tang J., Zhang Y., Xun X., Tang D., Peng D., Yi J., Liu Z., Shi X., 2014b. Synthesis and analgesic effects of μ-TRTX-Hhn1b on models of inflammatory and neuropathic pain. Toxins 6, 2363-2378.

Marrouchi R., Rome G., Kharrat R., Molgó J., Benoit E., 2013. Analysis of the action of gymnodimine-A and 13-desmethyl spirolide C on the mouse neuromuscular system *in vivo*. Toxicon 75, 27-34.

Mills S., Torrance N., Smith B.H., 2016. Identification and management of chronic pain in primary care: a review. Curr. Psychiatry Rep. 18, 22.

Molinski T.F., Dalisay D.S., Lievens S.L., Saludes J.P., 2009. Drug development from marine natural products. Nat. Rev. Drug Discov. 8, 69-86.

Namadurai S., Yereddi N.R., Cusdin F.S., Huang C.L., Chirgadze D.Y., Jackson A.P., 2015. A new look at sodium channel β subunits. Open Biol. 5, 140192.

Nature Outlook: Pain, 2016. Nature 535, S1-S48.

Netirojjanakul C., Miranda L.P., 2017. Progress and challenges in the optimization of toxin peptides for development as pain therapeutics. Curr. Opin. Chem. Biol. 38, 70-79.

Osteen J.D., Herzig V., Gilchrist J., Emrick J.J., Zhang C., Wang X., Castro J., Garcia-Caraballo S., Grundy L., Rychkov G.Y., Weyer A.D., Dekan Z., Undheim E.A., Alewood P., Stucky C.L., Brierley S.M., Basbaum A.I., Bosmans F., King G.F., Julius D., 2016. Selective spider toxins reveal a role for the NaV1.1

714 channel in mechanical pain. Nature 534, 494-499.
715 Peng K., Shu Q., Liu Z., Liang S., 2002. Function and solution structure of
716 huwentoxin-IV, a potent neuronal tetrodotoxin (TTX)-sensitive sodium channel
717 antagonist from Chinese bird spider *Selenocosmia huwena*. J Biol Chem. 277,
718 47564-47571.
719 Rahnama S., Deuis J.R., Cardoso F.C., Ramanujam V., Lewis R.J., Rash L.D., King
720 G.F., Vetter I., Mobli M., 2017. The structure, dynamics and selectivity profile of
721 a NaV1.7 potency-optimised huwentoxin-IV variant. PLoS ONE, 12, e0173551.
722 Rush A.M., Cummins T.R., Waxman S.G., 2007. Multiple sodium channels and their
723 roles in electrogenesis within dorsal root ganglion neurons. J. Physiol. Lond.
724 579, 1-14.
725 Saez N.J., Senff S., Jensen J.E., Er S.Y., Herzig V., Rash L.D., King G.F., 2010.
726 Spider-venom peptides as therapeutics. Toxins 2, 2851-2871.
727 Schlumberger S., Kristan K.C., Ota K., Frangež R., Molgó J., Sepčić K., Benoit E.,
728 Maček P., 2014. Permeability characteristics of cell-membrane pores induced
729 by ostreolysin A/pleurotolysin B, binary pore-forming proteins from the oyster
730 mushroom. FEBS Lett. 588, 35-40.
731 Schlumberger S., Ouanounou G., Girard E., Sasaki M., Fuwa H., Louzao M.C.,
732 Botana L.M., Benoit E., Molgó J., 2010. The marine polyether gambierol
733 enhances muscle contraction and blocks a transient K(+) current in skeletal
734 muscle cells. Toxicon 56, 785-791.
735 Schmidt G., 2010. Wie lautet der korrekte Name von Selenocosmia huwena Wang,
736 Peng & Xie, 1993?. Tarantulas of the World 142, 23-27.
737 Tsukamoto T., Chiba Y., Wakamori M., Yamada T., Tsunogae S., Cho Y.,
738 Sakakibara R., Imazu T., Tokoro S., Satake Y., Adachi M., Nishikawa T., Yotsu-
739 Yamashita M., Konoki K., 2017. Differential binding of tetrodotoxin and its
740 derivatives to voltage-sensitive sodium channel subtypes (Nav1.1 to Nav1.7).
741 Br. J. Pharmacol. *in press*. doi: 10.1111/bph.13985.
742 Vetter I., Deuis J.R., Mueller A., Israel M.R., Starobova H., Zhang A., Rash L., Mobli
743 M., 2016. NaV 1.7 as a pain target – from gene to pharmacology. Pharmacol.
744 Ther. 172, 73-100.
745 Wang F., Yan Z., Liu Z., Wang S., Wu Q., Yu S., Ding J., Dai Q., 2016. Molecular
746 basis of toxicity of N-type calcium channel inhibitor MVIIA. Neuropharmacology

747 101, 137-145.
748 Xiao Y., Bingham J.P., Zhu W., Moczydlowski E., Liang S., Cummins T.R., 2008.
749 Tarantula huwentoxin-IV inhibits neuronal sodium channels by binding to
750 receptor site 4 and trapping the domain II voltage sensor in the closed
751 configuration. J Biol Chem. 283, 27300-27313.
752 Xiao Y., Blumenthal K., Cummins T.R., 2014. Gating-pore currents demonstrate
753 selective and specific modulation of individual sodium channel voltage-sensors
754 by biological toxins. Mol Pharmacol. 86, 159-167.
755 Xiao Y., Blumenthal K., Jackson J.O. 2nd, Liang S., Cummins T.R., 2010. The
756 tarantula toxins ProTx-II and huwentoxin-IV differentially interact with human
757 $Na_V1.7$ voltage sensors to inhibit channel activation and inactivation. Mol
758 Pharmacol. 78, 1124-1134.
759 Xiao Y., Jackson J.O. 2nd, Liang S., Cummins T.R., 2011. Common molecular
760 determinants of tarantula huwentoxin-IV inhibition of Na+ channel voltage
761 sensors in domains II and IV. J. Biol. Chem. 286, 27301-27310.
762 Xu Q., Huang K., Gao L., Zhang H., Rong K., 2003. Toxicity of tetrodotoxin towards
763 mice and rabbits. Wei Sheng Yan Jiu (Chinese) 32, 371-374.
764 Yekkirala A.S., Roberson D.P., Bean B.P., Woolf C.J., 2017. Breaking barriers to
765 novel analgesic drug development. Nat. Rev. Drug Discov. 16, 545-564.
766 Yu H., Liu H., Yan Y., Duan Z., Wang X., 2014. Detection and identification of
767 huwentoxin-IV interacting proteins by biotin-avidin chemistry combined with
768 mass spectrometry. J. Venom. Anim. Toxins Incl. Trop. Dis. 20, 18.
769

Table 1. Parameters of steady-state inactivation- ($V_{P50\%}$ and k_h) and conductance- ($V_{T50\%}$ and k_g) voltage relationships for HEK-293 cells overexpressing $hNa_V1.6$ and $hNa_V1.7$ channel subtypes (means ± S.D. of 4-5 cells) and mouse DRG neurons having TTX-S sodium current (means ± S.D. of 4 neurons).

	$V_{P50\%}$ (mV)	k_h (mV^{-1})	$V_{T50\%}$ (mV)	k_g (mV^{-1})
$hNa_V1.6$ current before HwTx-IV perfusion	-61 ± 3	5.7 ± 0.3	-20 ± 2	5.4 ± 0.4
$hNa_V1.6$ current after HwTx-IV perfusion[1]	-65 ± 2	5.9 ± 0.4	-22 ± 3	4.8 ± 0.4
$hNa_V1.7$ current before HwTx-IV perfusion	-76 ± 3	6.9 ± 0.3	-21 ± 2	5.6 ± 0.5
$hNa_V1.7$ current after HwTx-IV perfusion[2]	-79 ± 3	7.4 ± 0.6	-22 ± 2	6.6 ± 0.5
TTX-S current before HwTx-IV perfusion	-80 ± 2	7.0 ± 0.6	-38 ± 4	3.7 ± 1.4
TTX-S current after HwTx-IV perfusion[3]	-86 ± 7	6.3 ± 0.5	-38 ± 3	4.4 ± 1.7

[1] 70-100 nM, [2] 20 nM, and [3] 0.1 µM.

Table 2. Kinetics parameters of current activation (tp) and inactivation (τh) calculated from TTX-S and TTX-R sodium currents recorded from DRG neurons under the indicated conditions (means ± S.D. of 4-12 cells).

	tp (ms)	**τh** (ms)
TTX-S current before TTX perfusion[1]	1.22 ± 0.29	0.78 ± 0.40
TTX-S current after TTX wash-out	0.81 ± 0.04	0.63 ± 0.18
TTX-S current after HwTx-IV perfusion[2]	0.75 ± 0.06	0.60 ± 0.12
TTX-R current before TTX perfusion	2.31 ± 0.62*	1.11 ± 0.24*

[1] 100 nM, [2] 0.1 µM. *: $P \leq 0.032$ (*versus* TTX-S current before TTX perfusion).

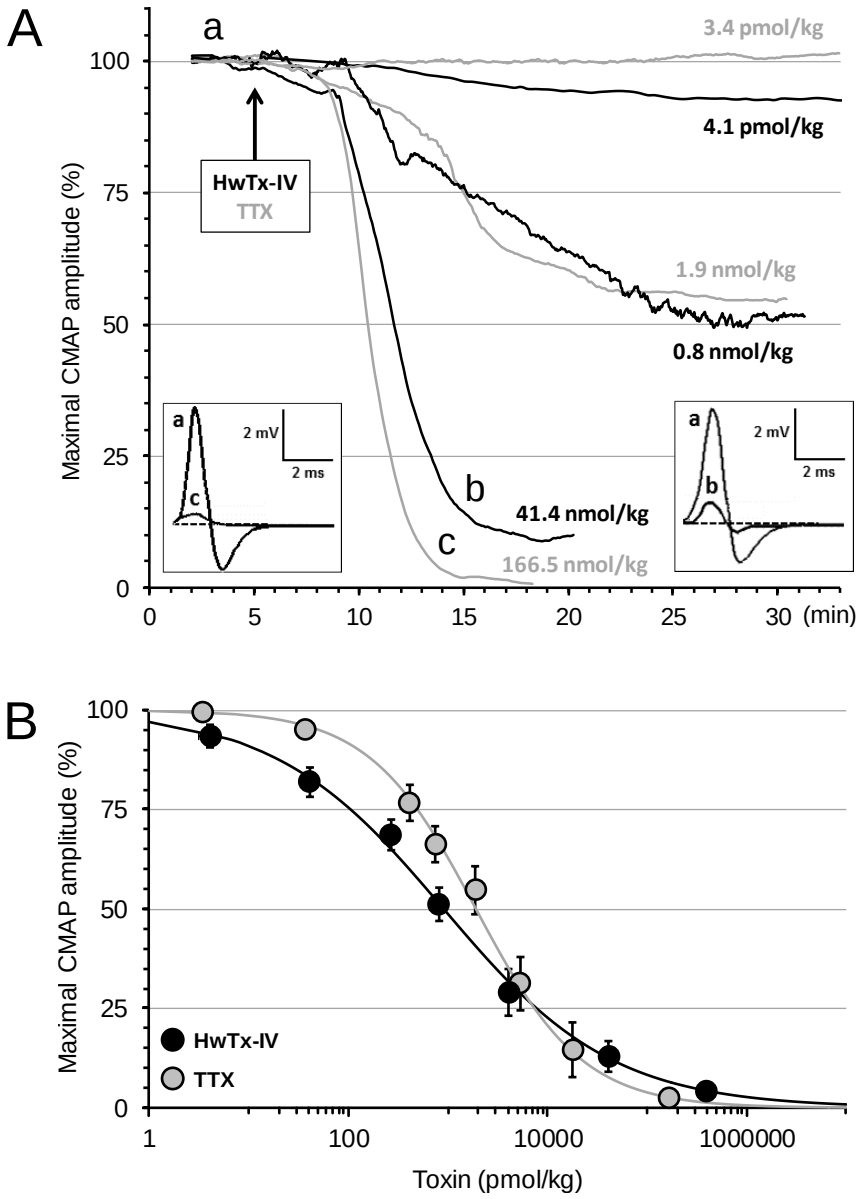

Fig. 1. Effects of HwTx-IV and TTX on the maximal CMAP amplitude recorded *in vivo* from mouse tail muscle in response to caudal motor nerve stimulation. **A**: Representative time-course of the effects of HwTx-IV (from 4.1 pmol/kg to 41.4 nmol/kg mouse, in black) and TTX (from 3.4 pmol/kg to 166.5 nmol/kg mouse, in grey) on the maximal CMAP amplitude recorded continuously as a function of time. Values are expressed as percentage of those before injections (indicated by the arrow). **Insets**: Superimposed traces of maximal CMAP, before (**a**) and ~10 min after HwTx-IV (41.4 nmol/kg mouse, **b**) or TTX (166.5 nmol/kg mouse, **c**) injection. **B**: Concentration-response curves of the effects of HwTx-IV (black circles) and TTX (grey circles) on the maximal CMAP amplitude. Each value, expressed as percentage of that obtained before injection, represents the mean ± S.D. of data obtained from 4-8 mice. IC_{50} and n_H values were, respectively, 0.9 nmol/kg mouse and 0.5 for HwTx-IV ($r^2 = 0.998$) and 1.9 nmol/kg mouse and 0.8 for TTX ($r^2 = 0.997$).

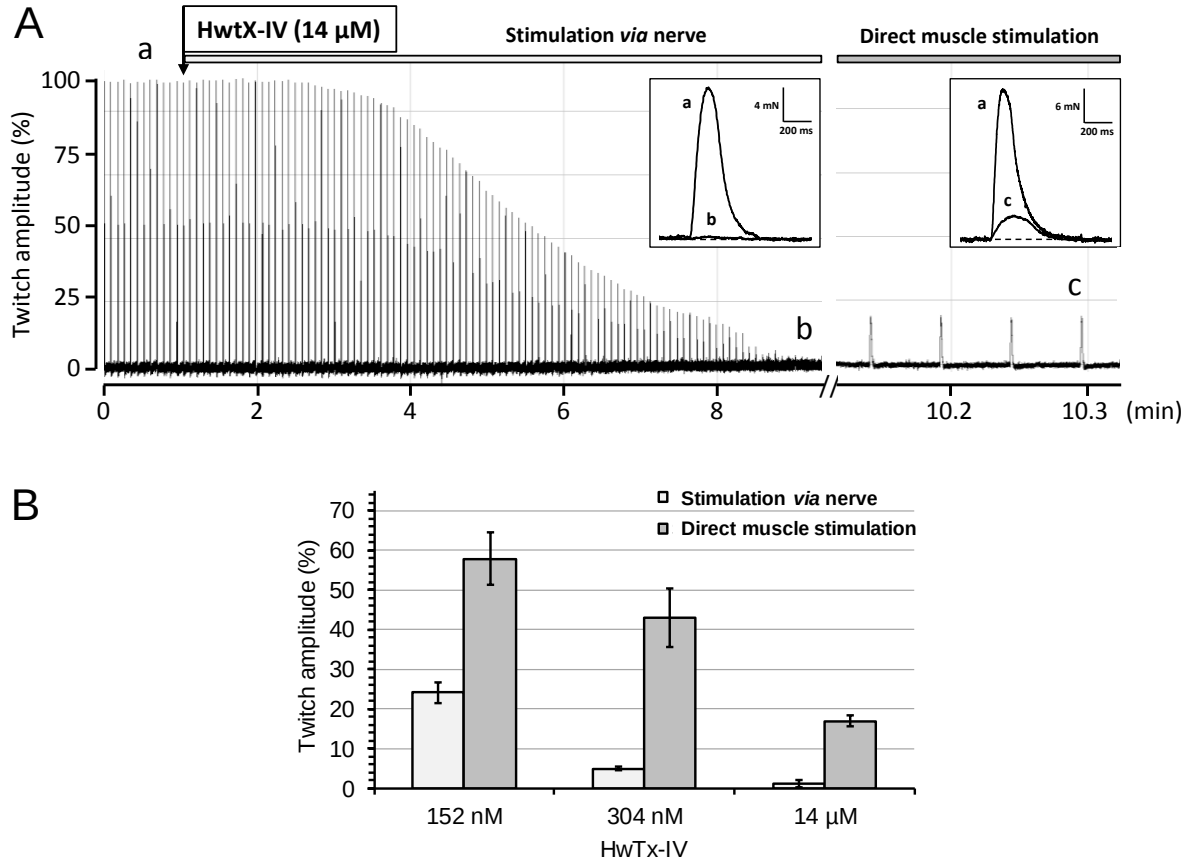

Fig. 2. Effects of HwTx-IV on nerve-evoked and directly-elicited muscle contractile force (single twitch) of isolated mouse phrenic nerve-hemidiaphragm preparation. **A**: Representative time-course of HwTx-IV (14 µM) effects on the maximal twitch amplitude recorded continuously as a function of time, and expressed as percentage of that before toxin addition to the standard physiological medium (indicated by the arrow), in response to stimulation applied either indirectly *via* the motor nerve (light grey) or directly to muscle (dark grey). **Insets**: Superimposed traces of maximal twitch recorded before (**a**) and ~10 min after HwTx-IV (14 µM) addition to the standard physiological medium (**b** and **c**), and elicited *via* nerve stimulation (**b**) or by direct muscle stimulation (**c**). **B**: Histogram representing nerve-evoked (light grey) and directly-elicited muscle (dark grey) maximal twitch amplitude determined in the presence of indicated HwTx-IV concentrations. Each value, expressed as percentage of that obtained before toxin addition to the standard physiological medium, represents the mean ± S.D. of data obtained from 4-10 muscles.

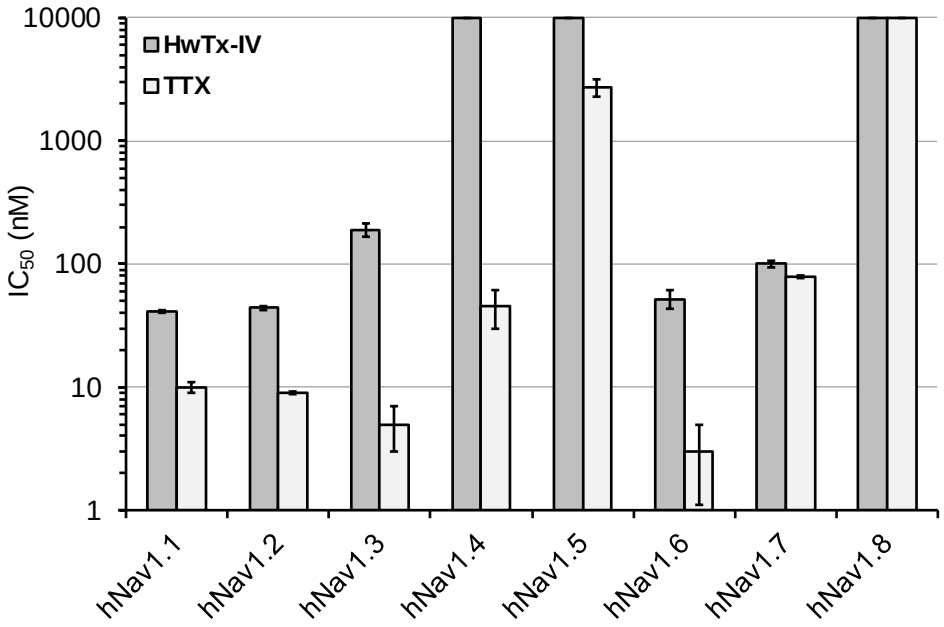

Fig. 3. Effects of HwTx-IV and TTX on HEK-293 cells overexpressing $hNa_V1.1$-1.8 channel subtypes. Histogram of IC_{50} values obtained from the concentration-response curves of HwTx-IV (dark grey) and TTX (light grey) effects on $hNa_V1.1$-1.8 currents. Each value represents the mean ± S.D. of data obtained from 2-10 cells. Mean values ± S.D. of n_H were 1.3 ± 0.2 and 1.0 ± 0.1 for HwTx-IV and TTX effects, respectively.

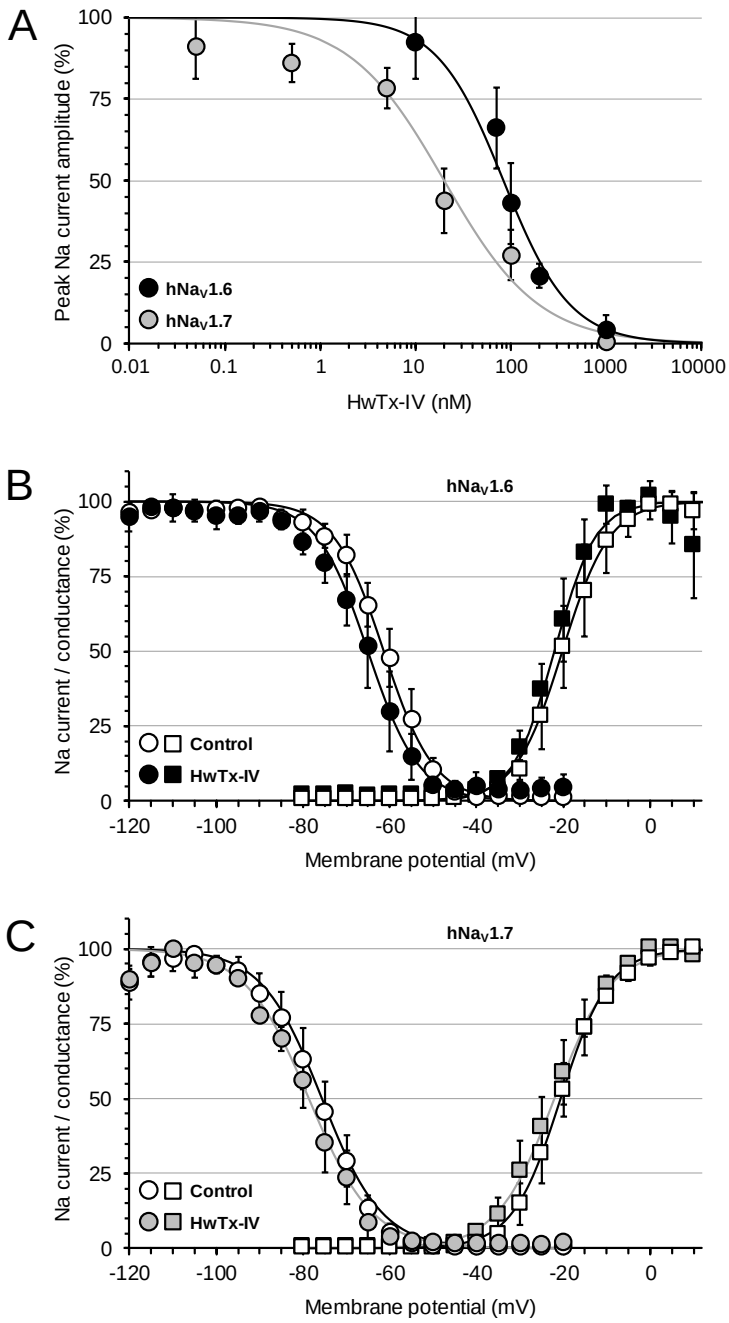

Fig. 4. Effects of HwTx-IV on HEK-293 cells overexpressing $hNa_V1.6$ and $hNa_V1.7$ channel subtypes. **A**: Concentration-response curves of HwTx-IV effects on $hNa_V1.6$ (black circles) and $hNa_V1.7$ (grey circles) currents. Each value, expressed as percentage of that obtained before toxin perfusion, represents the mean ± S.D. of data obtained from 4-9 cells. IC_{50} and n_H values were, respectively, 83.3 nM and 1.2 for $hNa_V1.6$ current (r^2 = 0.983), and 32.6 nM and 0.8 for $hNa_V1.7$ current (r^2 = 0.901). **B** and **C**: Steady-state inactivation- (circles) and conductance- (squares) voltage relationships for HEK-293 cells overexpressing $hNa_V1.6$ (**B**) and $hNa_V1.7$ (**C**) channel subtypes, before (open symbols) and after (close symbols) perfusion of 70-100 nM (**B**) or 20 nM (**C**) HwTx-IV. Each value represents the mean ± S.D. of data obtained from 4-5 cells, and is expressed as percentage of either maximal peak amplitude of current at large negative pre-pulse voltages or maximal conductance calculated at large positive test-pulse voltages. The theoretical curves correspond to data point fits with the mean $V_{P50\%}$, k_h, $V_{T50\%}$ and k_g values indicated in Table 1.

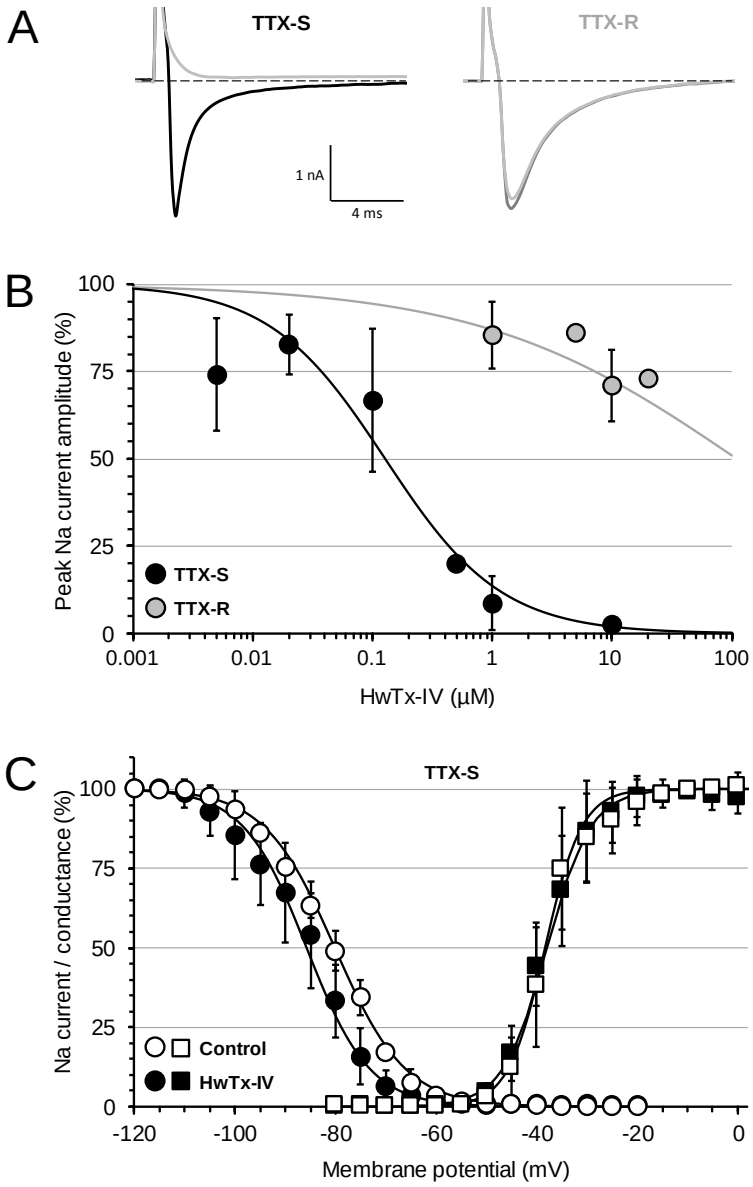

Fig. 5. Effects of HwTx-IV on TTX-S and TTX-R sodium currents of mouse DRG neurons. **A**: Representative traces of sodium currents recorded from two different neurons having either TTX-S (left) or TTX-R (right) current. In each case, the current was recorded before (black or dark grey) and 1 to 5 min after (light grey) perfusion of 100 nM TTX. **B**: Concentration-response curves of HwTx-IV effects on the peak amplitude of TTX-S (black circles) and TTX-R (grey circles) sodium currents. Each value, expressed as percentage of that obtained before toxin perfusion, represents the mean ± S.D. of data obtained from 2-9 neurons. IC_{50} and n_H values were, respectively, 0.13 µM and 0.9 for TTX-S current (r^2 = 0.967), and 110 µM and 0.4 for TTX-R current (r^2 = 0.612). **C**: Steady-state inactivation- (circles) and conductance- (squares) voltage relationships for neurons having TTX-S current, before (open symbols) and after (close symbols) perfusion of 0.1 µM HwTx-IV. Each value represents the mean ± S.D. of data obtained from 4 neurons, and is expressed as percentage of either maximal peak amplitude of current at large negative pre-pulse voltages or maximal conductance calculated at large positive test-pulse voltages. The theoretical curves correspond to data point fits with the mean $V_{P50\%}$, k_h, $V_{T50\%}$ and k_g values indicated in Table 1.

Direct evidence for high affinity blockade of NaV1.6 channel subtype by huwentoxin-IV spider peptide, using multiscale functional approaches

T.C. Gonçalves, R. Boukaiba, J. Molgó, M. Amar, M. Partiseti, D. Servent, and E. Benoit

SUPPLEMENTARY FIGURE 1

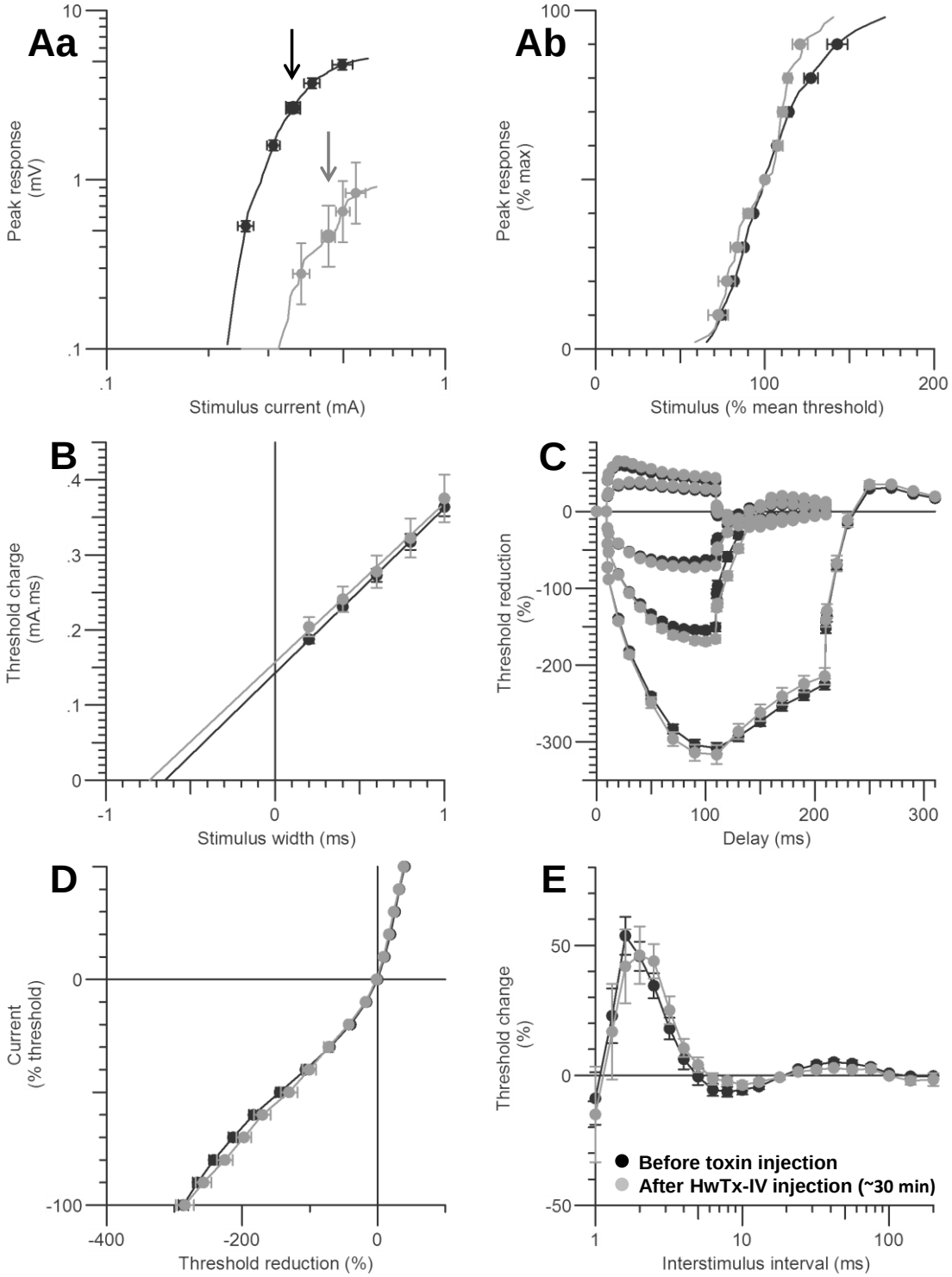

Figure S1. Superimposed excitability curves obtained *in vivo* by stimulating the mouse caudal motor nerve and recording the CMAP from tail muscle before (black circles, n = 29 mice) and ~30 min after injections of HwTx-IV (4.1-41.4 nmol/kg mouse, grey circles, n = 6 mice). Data are represented as means ± S.D. **A**: stimulus-response relationships [absolute (**a**) and relative (**b**) CMAP amplitudes], **B**: strength-duration relationship, **C**: threshold electrotonus, **D**: current-threshold relationship, and **E**: recovery cycle. In Aa, arrows indicate stimulus currents for 50% maximal response.

Direct evidence for high affinity blockade of NaV1.6 channel subtype by huwentoxin-IV spider peptide, using multiscale functional approaches
T.C. Gonçalves, R. Boukaiba, J. Molgó, M. Amar, M. Partiseti, D. Servent, and E. Benoit

SUPPLEMENTARY FIGURE 2

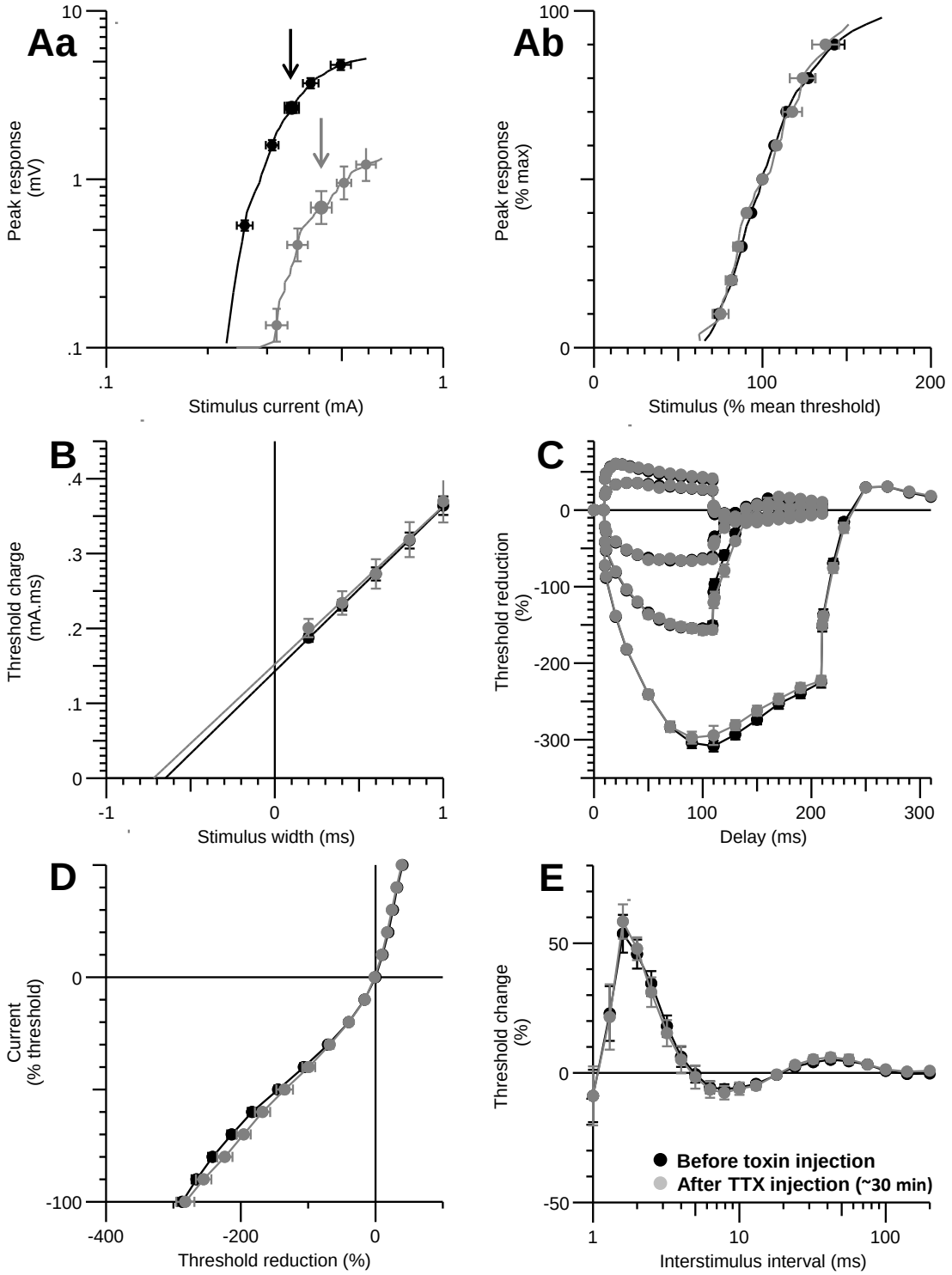

Figure S2. Superimposed excitability curves obtained *in vivo* by stimulating the mouse caudal motor nerve and recording the CMAP from tail muscle before (black circles, n = 29 mice) and ~30 min after injections of TTX (5.3-17.8 nmol/kg mouse, grey circles, n = 9 mice). Data are represented as means ± S.D. **A**: stimulus-response relationships [absolute (**a**) and relative (**b**) CMAP amplitudes], **B**: strength-duration relationship, **C**: threshold electrotonus, **D**: current-threshold relationship, and **E**: recovery cycle. In Aa, arrows indicate stimulus currents for 50% maximal response.

Direct evidence for high affinity blockade of NaV1.6 channel subtype by huwentoxin-IV spider peptide, using multiscale functional approaches

T.C. Gonçalves, R. Boukaiba, J. Molgó, M. Amar, M. Partiseti, D. Servent, and E. Benoit

SUPPLEMENTARY FIGURE 3

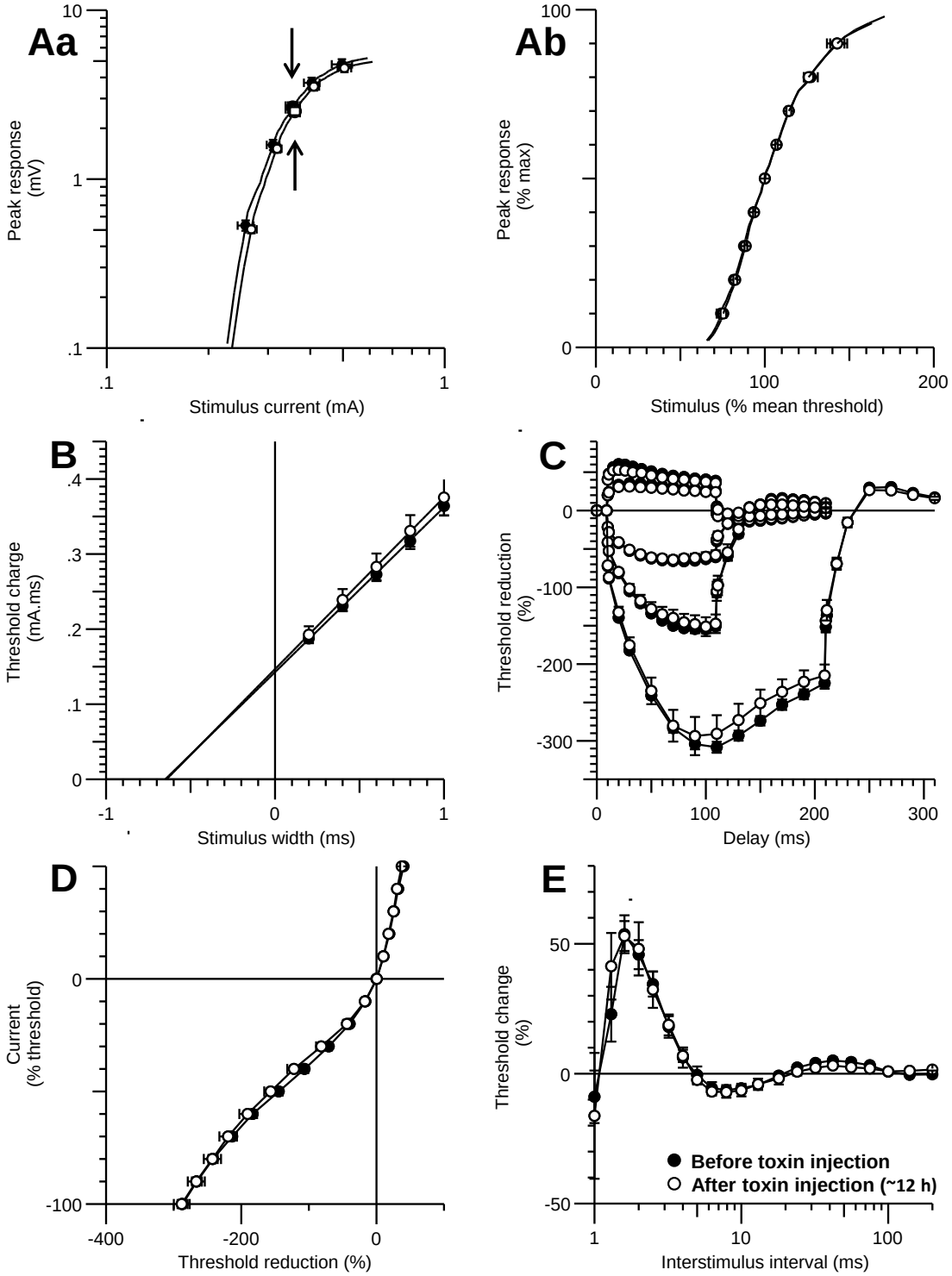

Figure S3. Superimposed excitability curves obtained *in vivo* by stimulating the mouse caudal motor nerve and recording the CMAP from tail muscle before (black circles, n = 29 mice) and ~12 h after injections (white circles, n = 12 mice) of HwTx-IV (4.1-41.4 nmol/kg mouse) or TTX (5.3-17.8 nmol/kg mouse). Data are represented as means ± S.D. **A**: stimulus-response relationships [absolute (**a**) and relative (**b**) CMAP amplitudes], **B**: strength-duration relationship, **C**: threshold electrotonus, **D**: current-threshold relationship, and **E**: recovery cycle. In Aa, arrows indicate stimulus currents for 50% maximal response.

Direct evidence for high affinity blockade of NaV1.6 channel subtype by huwentoxin-IV spider peptide, using multiscale functional approaches

T.C. Gonçalves, R. Boukaiba, J. Molgó, M. Amar, M. Partiseti, D. Servent, and E. Benoit

SUPPLEMENTARY TABLE 1

Table S1. Comparison of neuromuscular excitability parameters (means ± S.D.) from mouse tail muscle recordings before toxin injections (control, n = 29 mice), ~30 min after injections of HwTx-IV (4.1-41.4 nmol/kg mouse, n = 6 mice) or TTX (5.3-17.8 nmol/kg mouse, n = 9 mice), and ~12 h after toxin injections (n = 12 mice).

	Excitability parameter[2]	**Before toxin injection**	**~30 min after injection**		**~12 h after toxin injection**
			HwTx-IV	**TTX**	
A[1]	Peak response (mV)	5.31 ± 0.57	0.92 ± 0.31**	1.36 ± 0.25**	5.04 ± 0.56
A	Latency (ms)	3.89 ± 0.06	4.09 ± 0.26	4.09 ± 0.12	3.91 ± 0.04
A	Stimulus (mA) for 50% max response	0.35 ± 0.05	0.46 ± 0.05*	0.44 ± 0.08*	0.36 ± 0.06
A	Stimulus-response slope	3.11 ± 0.18	3.42 ± 0.17	2.96 ± 0.17	3.21 ± 0.16
B[1]	Strength-duration time constant (ms)	0.69 ± 0.12	0.86 ± 0.14	0.87 ± 0.11	0.66 ± 0.03
B	Rheobase (mA)	0.21 ± 0.04	0.19 ± 1.16	0.19 ± 0.03	0.22 ± 0.08
C[1]	TEd (10-20 ms, 40%)	59.53 ± 1.27	54.84 ± 1.58	59.19 ± 1.84	56.07 ± 2.07
C	TEd (peak, 40%)	59.00 ± 1.17	63.62 ± 1.43	60.52 ± 1.96	56.28 ± 1.92
C	TEd (peak, 20%)	35.81 ± 0.75	38.65 ± 1.69	36.14 ± 1.03	33.57 ± 1.53
C	TEd (40-60 ms, 40%)	47.92 ± 1.14	51.90 ± 1.09	50.17 ± 2.03	43.29 ± 2.29
C	TEd (90-100 ms, 40%)	39.52 ± 1.27	41.49 ± 1.25	42.20 ± 1.67	36.56 ± 2.41
C	Accommodation half-time (ms, 40%)	46.02 ± 0.93	44.09 ± 1.15	46.05 ± 1.70	45.16 ± 2.69
C	S2 accommodation	19.48 ± 0.77	19.13 ± 1.32	18.32 ± 0.89	18.72 ± 1.45
C	TEd (undershoot, 40%)	-15.34 ± 1.01	-12.26 ± 1.27	-17.67 ± 1.35	-13.43 ± 1.29
C	TEh (10-20 ms, -40%)	-93.31 ± 1.12	-94.49 ± 1.56	-91.87 ± 2.14	-90.88 ± 4.93
C	TEh (20-40 ms, -40%)	-120.1 ± 1.9	-124.0 ± 3.0	-119.8 ± 3.4	-116.2 ± 7.5
C	TEh (90-100 ms, -40%)	-152.7 ± 5.2	-167.9 ± 4.9	-156.7 ± 5.6	-149.4 ± 12.1
C	TEh (slope 101-140 ms, -40%)	2.62 ± 0.17	2.74 ± 0.11	2.93 ± 0.20	2.60 ± 0.30
C	TEh (peak, -70%)	-312.4 ± 6.7	-321.8 ± 11.0	-300.3 ± 10.1	-297.8 ± 22.8
C	S3 (-70%)	80.28 ± 6.98	102.1 ± 11.4	80.48 ± 7.91	78.85 ± 11.20
C	TEh (overshoot, -40%)	17.33 ± 1.05	20.23 ± 1.41	17.70 ± 1.20	15.62 ± 1.71
D[1]	Resting slope	0.89 ± 0.09	0.86 ± 0.12	0.89 ± 0.11	0.96 ± 0.26
D	Minimum slope	0.23 ± 0.01	0.23 ± 0.02	0.23 ± 0.02	0.24 ± 0.02
D	Hyperpolarization slope	0.49 ± 0.03	0.39 ± 0.05	0.40 ± 0.06	0.48 ± 0.05
E[1]	Refractoriness at 2 ms (%)	45.82 ± 5.60	46.20 ± 11.00	47.91 ± 4.41	48.05 ± 10.20
E	Refractoriness at 2.5 ms (%)	34.48 ± 4.78	43.90 ± 6.62	31.13 ± 5.72	32.36 ± 7.01
E	Relative refractory period (ms)	4.38 ± 1.09	5.05 ± 1.22	4.36 ± 1.11	4.70 ± 1.07
E	Superexcitability (%)	-19.00 ± 3.91	-23.53 ± 8.01	-17.94 ± 3.74	-9.00 ± 3.17
E	Superexcitability at 5 ms (%)	-0.49 ± 3.26	3.98 ± 2.84	-1.63 ± 4.46	-2.40 ± 1.75
E	Superexcitability at 7 ms (%)	-5.94 ± 2.06	-1.78 ± 1.69	-7.06 ± 2.83	-7.01 ± 1.76
E	Subexcitability (%)	5.60 ± 1.09	3.29 ± 0.85	6.61 ± 1.46	2.93 ± 0.64

[1] A: stimulus-response relationship, B: strength-duration relationship, C: threshold electrotonus, D: current-threshold relationship, and E: recovery cycle. [2] TEd: threshold electrotonus from depolarizing currents and TEh: threshold electrotonus from hyperpolarizing currents. Differences (*versus* control), considered to be significant at $P \leq 0.05$ (*: $P \leq 0.032$, **: $P \leq 9.4 \times 10^{-8}$), are highlighted in grey.